Supporting Information for **"Largely enhanced bulk photovoltaic effects in the two-dimensional $MoSi_2N_4$ monolayer photodetector by vacancy-doping and bending-increased device asymmetry"**

by Tingting Duan, Yongsheng Yao, Juexian Cao, Xiaolin Wei

In this supporting information, we provide useful supporting information concerning (1) The unit cell of α_1- and α_2-$MoSi_2N_4$; (2) The lattice, band gaps, and band gap types of α_1- and α_2-$MoSi_2N_4$; (3) The bandstructure and density of states of α_1-and α_2-$MoSi_2N_4$; (4) The projected density of states of α_1-and α_2-$MoSi_2N_4$; (5) The photocurrent for the photodetector with the four different vacancies center regions of α_2-$MoSi_2N_4$, respectively; (6) The photocurrent for the photodetector with the three different bending angles center regions of α_2-$MoSi_2N_4$, respectively; (7) The I_{max} and ER of vacancies center region of α_2-$MoSi_2N_4$, respectively; (8) The I_{max} and ER of bending angle center region of α_2-$MoSi_2N_4$, respectively; (9) The electronic transmission spectrum of vacancies center region of α_2-$MoSi_2N_4$; (10) The electronic transmission spectrum of bending center region of α_2-$MoSi_2N_4$; (11) The I_{max} of N-vacancies and bending angle with 20º center region of α_2-$MoSi_2N_4$.

(1) The unit cell of α_1- and α_2 $MoSi_2N_4$

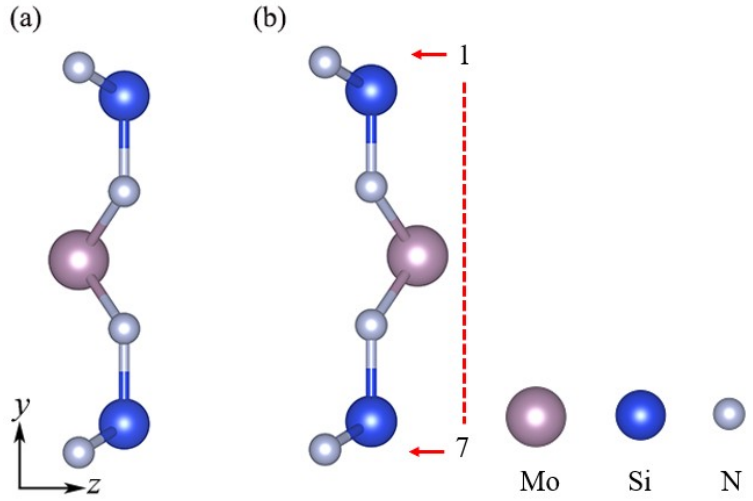

Fig. S1 The structure of α_1-$MoSi_2N_4$ and (b) α_2-$MoSi_2N_4$ unit cell, the grayish purple, blue, and gray-blue atoms represent the Mo, Si, and N atoms, respectively.

(2) The lattice, band gaps, and band gap types of α_1- and α_2-$MoSi_2N_4$

Table S1. Lattice constants, PBE band gaps, and band gap types of $MoSi_2N_4$ in α_1 and α_2 phases.

Structure	a (Å)	c (Å)	E_g (eV)	Band type	E_g (Ref[47])	E_g (Ref[4])	E_g (Ref[10])
α_1-$MoSi_2N_4$	2.90	2.51	1.86	Indirect	/	/	Indirect (1.74)
α_2-$MoSi_2N_4$	2.89	2.50	2.10	Indirect	Indirect (2.06)	Indirect (2.02)	/

(3) The bandstructure and density of states of α_1-and α_2-$MoSi_2N_4$

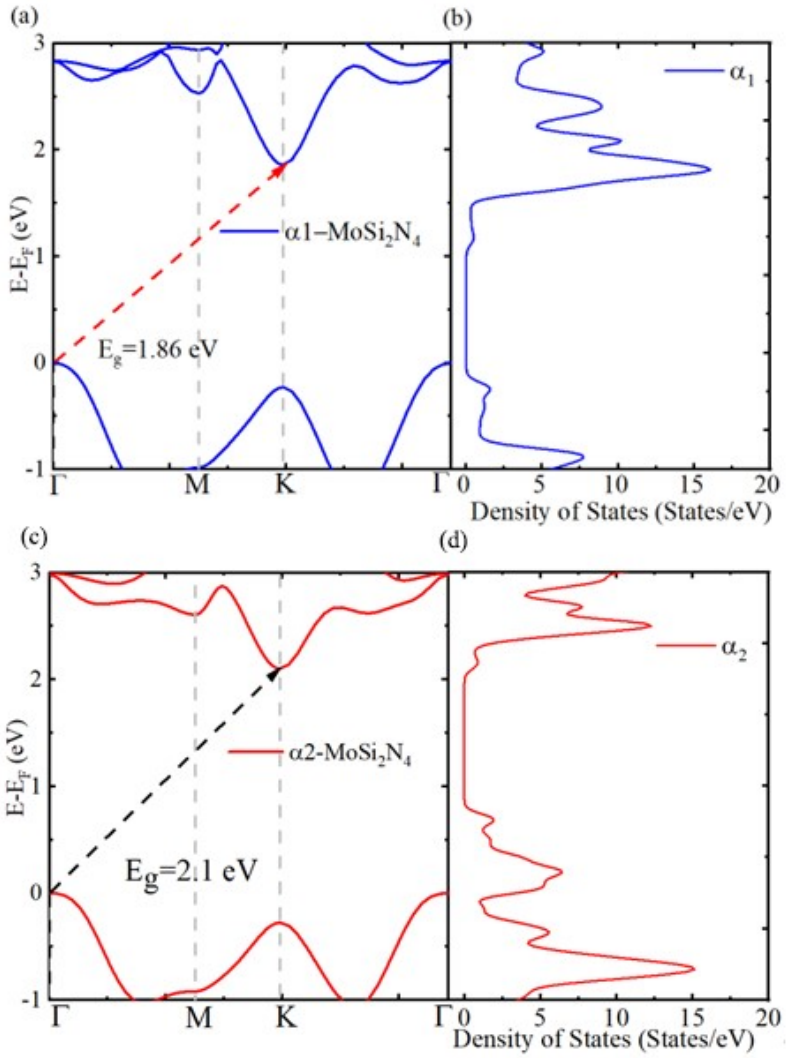

Fig. S2 (a)-(d) are the bandstructure and density of states of α_1-and α_2-$MoSi_2N_4$, respectively.

(4) The projected density of states of α_1-and α_2-$MoSi_2N_4$

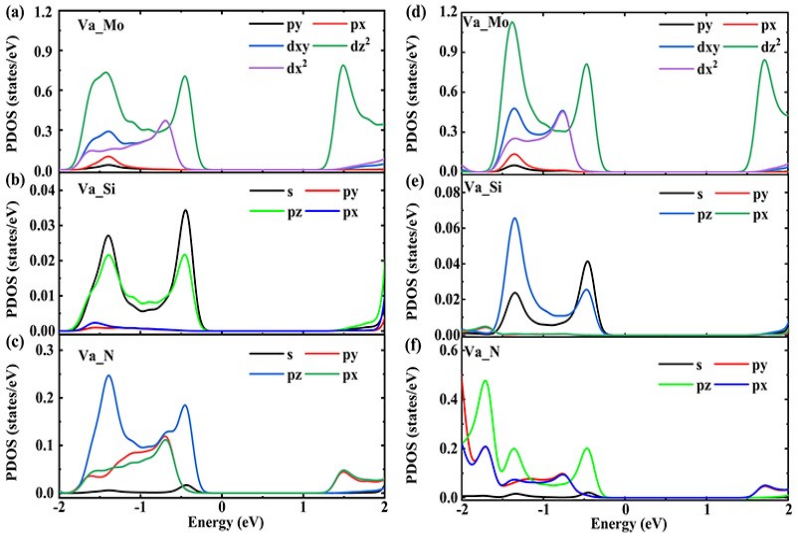

Fig. S3 (a) and (b) are the PDOS of α_1 and α_2-$MoSi_2N_4$, respectively.

(5) The photocurrent for the photodetector with the four different vacancies center regions of α_2-$MoSi_2N_4$, respectively.

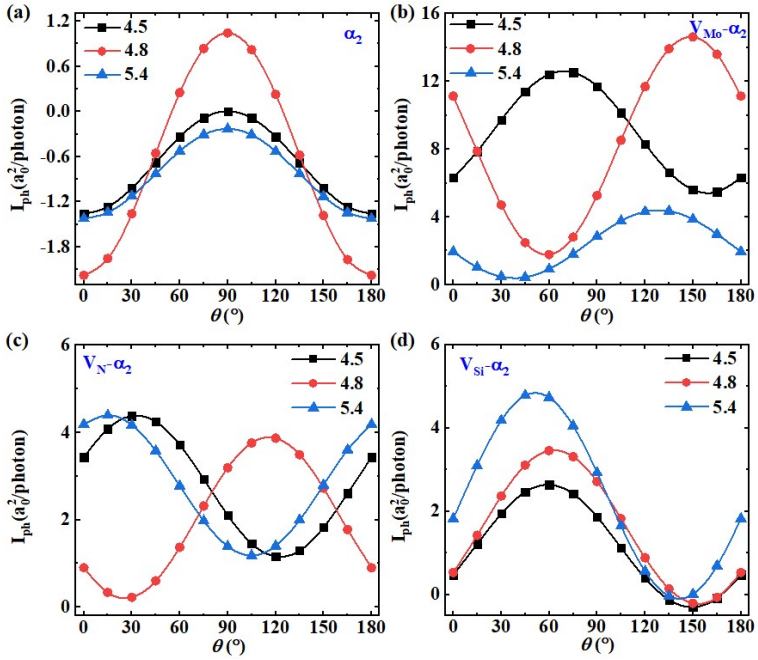

Fig. S4 (a)-(d) are the photocurrent at the photon energy of 4.5 eV, 4.8 eV, and 5.4 eV for the photodetector with the four different center regions of α_2-$MoSi_2N_4$, respectively.

(6) The photocurrent for the photodetector with the three different bending angles center regions of α_2-$MoSi_2N_4$, respectively.

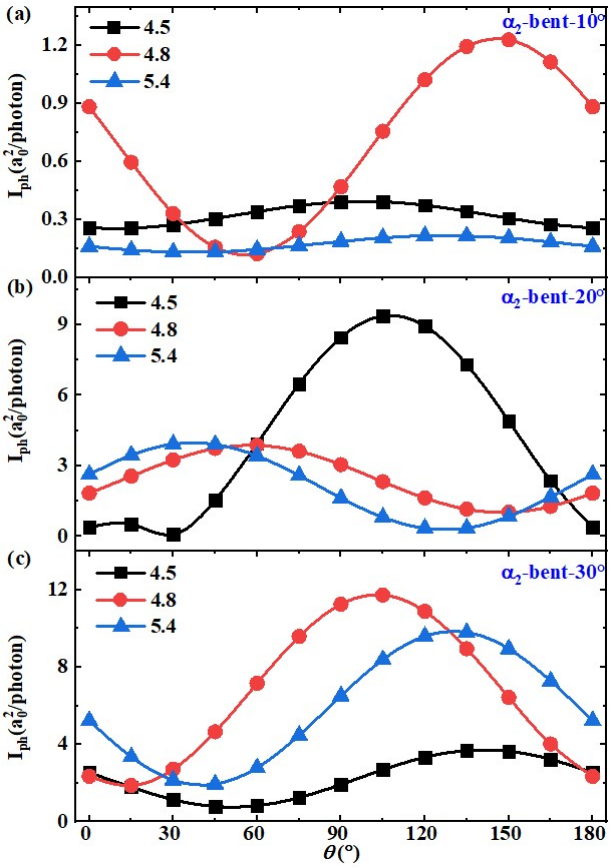

Fig. S5 (a)-(c) are the photocurrent at the photon energy of 4.5 eV, 4.8 eV, and 5.4 eV for the photodetector with the three different bending angles center regions of α_2-$MoSi_2N_4$, respectively.

(7) The I_{max} and ER of vacancies center region α_2-$MoSi_2N_4$.

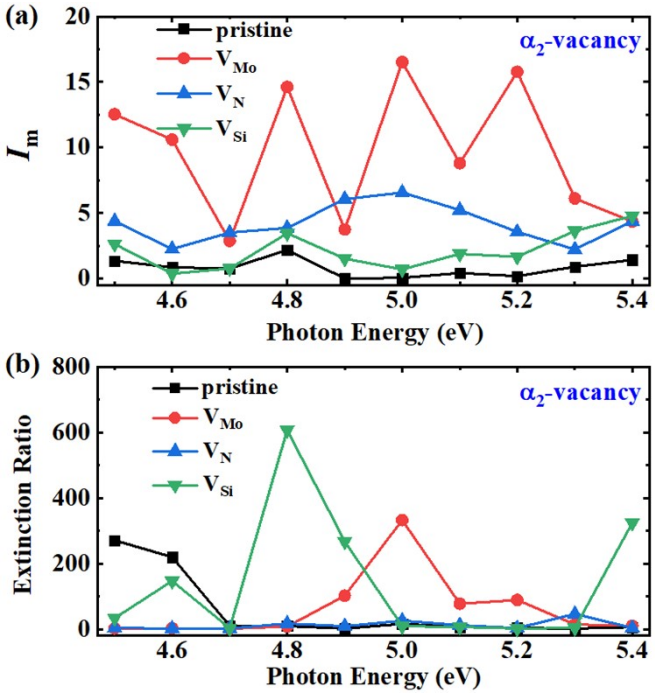

Fig. S6 (a) The maximum of photocurrent and (b) extinction ratio of α_2-$MoSi_2N_4$.

(8) The I_{max} and ER of bending angle center regions α_2-$MoSi_2N_4$.

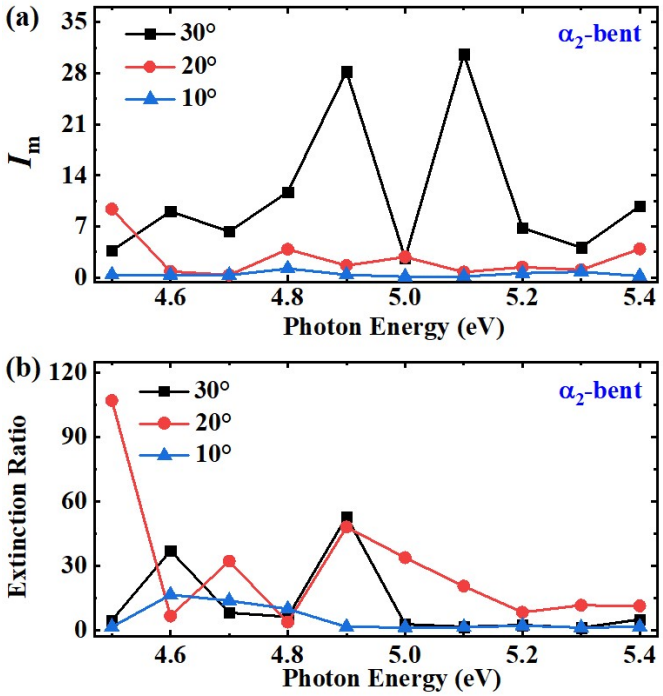

Fig. S7 (a) The maximum of photocurrent and (b)extinction ratio of α_2-$MoSi_2N_4$.

(9) The electronic transmission spectrum of vacancy center region of α_2-$MoSi_2N_4$.

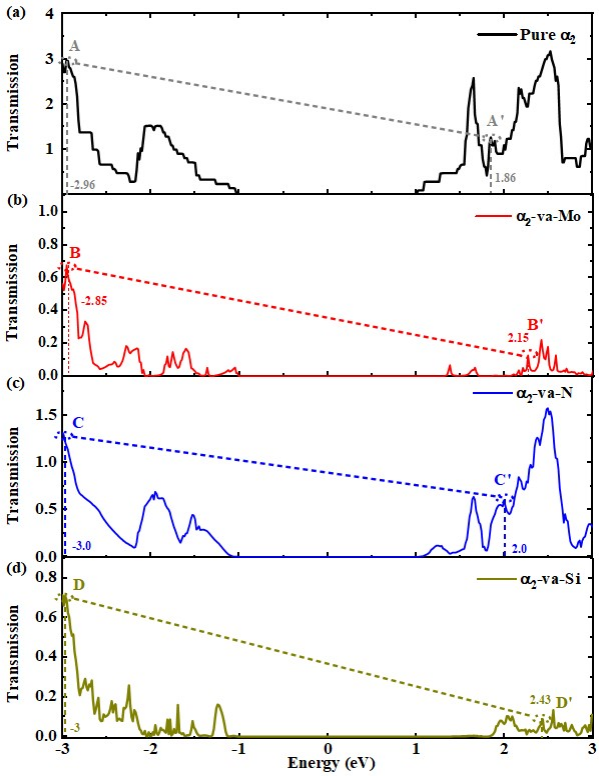

Fig. S8 (a) Electron transmission spectra of α_2-$MoSi_2N_4$ monolayer devices with (a) defect-free, (b) Mo-defect, (c) N-defect, and (d) Si-defect systems.

(10) The electronic transmission spectrum of bending center region of α_2-$MoSi_2N_4$.

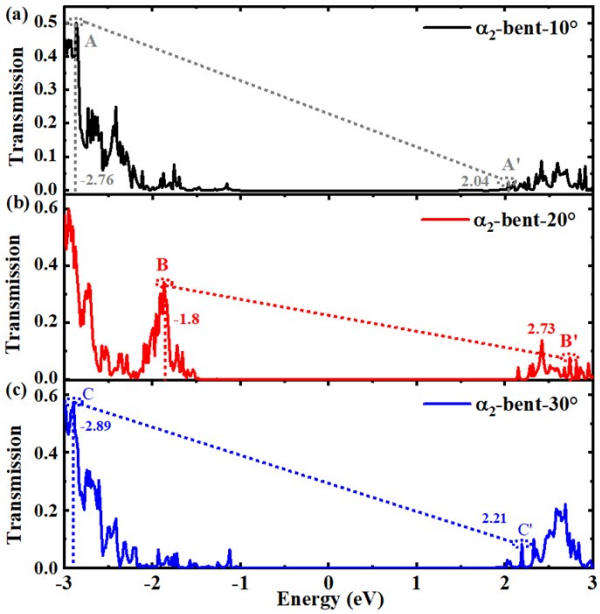

Fig. S9 (a) Electron transmission spectra of α_2-$MoSi_2N_4$ monolayer devices with bending angle of (a) 10º, (b) 20º, and (c) 30º, respectively.

(11) The I_{max} of N-vacancies and bending angle with 20º center region α_1-$MoSi_2N_4$.

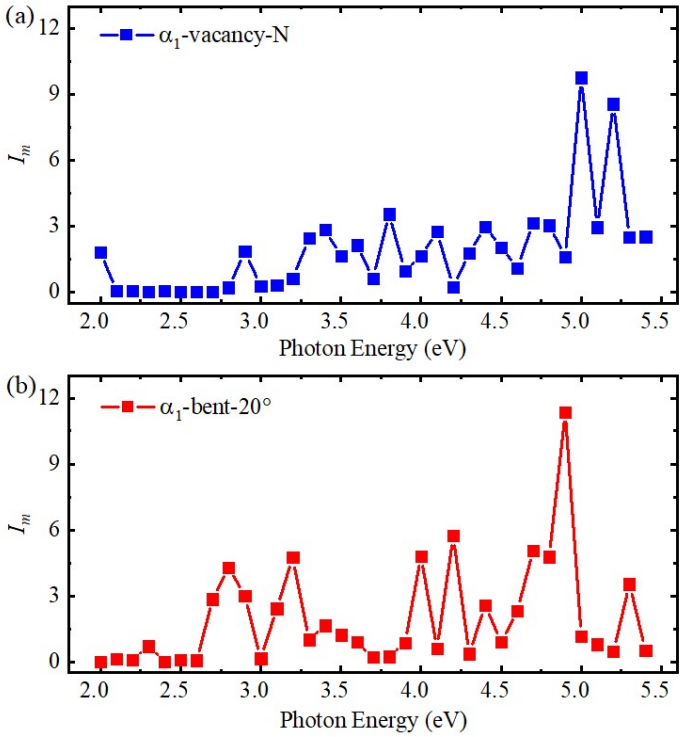

Fig. S10 (a) The maximum photocurrent of N-vacancy and (b) bending angle with 20º of α_1-$MoSi_2N_4$.